Accurate Gauge-Invariant Tensor Network Simulations for Abelian Lattice Gauge Theory in (2+1)D: Ground State and Real-time Dynamics

Yantao Wu[1,*] and Wen-Yuan Liu[2,†]

[1] *Institute of Physics, Chinese Academy of Sciences, Beijing 100190, China*
[2] *Institute for Advanced Study in Physics, Zhejiang University, Hangzhou 310027, China*

Supplemental Material

S-1. Variational Monte Carlo

There are standard works about the variational Monte Carlo algorithm for tensor network states [1–4]. It has been used in generic bosonic PEPS and fermionic PEPS for solving frustrated spin and fermionic models [5–17], as well as gauged Guassian PEPS for lattice gauge theories [4, 18–20]. Here we follow the presentation for generic PEPS in Ref. [5, 7], and discuss its application for gauge-invariant PEPS.

In VMC, using $|\mathbf{s}\rangle \equiv |\mathbf{n}, \mathbf{p}\rangle$ to denote gauge field configuration $|\mathbf{n}\rangle$ and matter field configuration $|\mathbf{p}\rangle$, the expectation values are computed by importance sampling of configurations $|\mathbf{s}\rangle$. For example, the total energy reads:

$$E_{\text{tot}} = \frac{\langle\Psi|H|\Psi\rangle}{\langle\Psi|\Psi\rangle} = \sum_{\mathbf{s}} \frac{|\langle \mathbf{s}\,|\Psi\rangle\,|^2}{\langle\Psi|\Psi\rangle} \frac{\langle \mathbf{s}|\,H|\Psi\rangle}{\langle \mathbf{s}|\,\Psi\rangle} = \sum_{\mathbf{s}} p(\mathbf{s}) E_{\text{loc}}(\mathbf{s}) \quad , \tag{S1}$$

where $\Psi(\mathbf{s}) \equiv \langle \mathbf{s}|\,\Psi\rangle$ is the amplitude of the configuration $|\mathbf{s}\rangle$, and $p(\mathbf{s}) = |\langle \mathbf{s}\,|\Psi\rangle\,|^2/\langle\Psi|\Psi\rangle$ is the probability. $E_{\text{loc}}(\mathbf{s})$ is the local energy defined as

$$E_{\text{loc}}(\mathbf{s}) = \frac{\langle \mathbf{s}|\,H|\Psi\rangle}{\langle \mathbf{s}|\,\Psi\rangle} = \sum_{\mathbf{s}'} \frac{\langle \mathbf{s}'|\,\Psi\rangle}{\langle \mathbf{s}|\,\Psi\rangle} \langle \mathbf{s}|\,H\,|\mathbf{s}'\rangle\,. \tag{S2}$$

The sampling process in Eq.(S1) employs the conventional Markov Chain Monte Carlo (MCMC) method. Beginning with the initial configuration $|\mathbf{s}_0\rangle$, a trial configuration $|\mathbf{s}_1\rangle$ is proposed. According to the Metropolis algorithm, this candidate configuration $|\mathbf{s}_1\rangle$ is accepted as the new configuration for the Markov Chain if a uniformly random number in [0,1) is below the probability ratio $p(\mathbf{s}_1)/p(\mathbf{s}_0)$. If rejected, another configuration state $|\mathbf{s}_1'\rangle$ is proposed instead.

Monte Carlo sampling provides a direct framework for calculating energy gradients to be used for updating variational parameter α_m of the wave function:

$$g_m = \langle O_m^*(\mathbf{s}) E_{\text{loc}}(\mathbf{s})\rangle - \langle O_m^*(\mathbf{s})\rangle\langle E_{\text{loc}}(\mathbf{s})\rangle, \tag{S3}$$

where $\langle ...\rangle$ means the Monte Carlo average, and $O_m^*(\mathbf{s}) = \frac{1}{\Psi^*(\mathbf{s})}\frac{\partial\Psi^*(\mathbf{s})}{\partial\alpha_m^*}$. This enables efficient wavefunction optimization via stochastic gradient descent or stochastic reconfiguration. Detailed implementations are discussed in Refs. [5, 7, 14].

A critical feature of VMC arises from the *zero energy variance principle* for ground states. For energy eigenstates, i.e. $H\,|\Psi\rangle = E_g\,|\Psi\rangle$, the energy variance $\text{var}\,\langle H\rangle = \langle H^2\rangle - \langle H\rangle^2 = 0$. In the context of Monte Carlo sampling, for energy eigenstates it has $E_{\text{loc}}(\mathbf{s}) = \langle \mathbf{s}|\,H|\Psi\rangle/\langle \mathbf{s}|\,\Psi\rangle = E_g$, which is independent of configurations $|\mathbf{s}\rangle$. Near the ground state, this property allows accurate energy estimation with minimal sampling noise, even using small sample sizes [21]. This is indeed what we observe, for example, in the comparison between PEPS and QMC results for the pure $\mathbb{Z}_2$ LGT presented in the main text.

S-2. VMC for gauge-invariant PEPS

Below we outline key considerations for implementing variational Monte Carlo (VMC) with gauge-invariant PEPS, focusing on amplitude computation and Markov chain configuration sampling.

Amplitude computations. The gauge-invariant PEPS $|\Psi\rangle$ inherently eliminates unphysical configurations: Any configuration $|\bar{\mathbf{s}}\rangle$ violating the gauge symmetry has $\langle\bar{\mathbf{s}}|\,\Psi\rangle = 0$, enforced by the block-sparse structure of PEPS tensors. For physical configurations $|\mathbf{s}\rangle \equiv |\mathbf{n}, \mathbf{p}\rangle$, considering the gauge canonical form, the gauge constraint requires

$$\text{mod}(p + n_l + n_d - n_u - n_r, N) = Q_{\text{x}} \tag{S4}$$

at each vertex $\mathbf{x}$ for $\mathbb{Z}_N$ gauge group, where p denotes matter configuration, and n_l, n_u, n_r, n_d represent gauge configurations on adjacent links..

The amplitude $\langle \mathbf{s}| \Psi\rangle$ for a physical configuration $|\mathbf{s}\rangle \equiv |\mathbf{n}, \mathbf{p}\rangle$ corresponds to a tensor network:

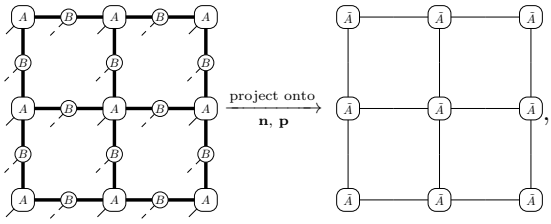

(S5)

where gauge symmetry reduces each tensor A to a single sector $\tilde{A}$, with B absent due to gauge canonical form. This reduces the bond dimension of amplitude networks to D_k, compared to the full PEPS bond dimension $D = \sum_k D_k$. The amplitude network are efficiently contracted using standard methods like SVD or variational compression [22].

Configuration sampling. The sampling starts by randomly selecting an initial configuration $|\mathbf{s}_0\rangle$ that satisfy the gauge constraint: For every vertex $\mathbf{x}$ in the $\mathbb{Z}_N$ gauge theory, the condition $\mathrm{mod}(p + n_l + n_d - n_u - n_r, N) = Q_{\mathbf{x}}$ must hold. To generate a trial gauge configuration $|\mathbf{s}_1\rangle$, the plaquette operator $P_{\mathrm{x}} = U_{\mathbf{x},1} U_{\mathbf{x}+\mathbf{e}_1,2} U^\dagger_{\mathbf{x}+\mathbf{e}_2,1} U^\dagger_{\mathbf{x},2}$ is applied to $|\mathbf{s}_0\rangle$, yielding $|\mathbf{s}_1\rangle = P^t_{\mathrm{x}} |\mathbf{s}_0\rangle$, where t is an random integer in $[1, N-1]$ for $\mathbb{Z}_N$ gauge group. This procedure inherently preserves the gauge constraint, ensuring $|\mathbf{s}_1\rangle$ remains physical. The Metropolis algorithm (as described previously) then determines whether $|\mathbf{s}_1\rangle$ is accepted into the Markov chain. For systems with dynamic matter fields, local updates are additionally performed on both gauge and matter configurations living on links, following $|\mathbf{s}_1\rangle = c^\dagger_{\mathbf{x}} U_{(\mathbf{x},\alpha)} c_{\mathbf{x}+\mathbf{e}_\alpha} |\mathbf{s}_0\rangle$.

To accelerate sampling, all plaquettes and links are updated sequentially rather than randomly. This approach significantly reduces computational costs from $O(N^2_{\mathrm{site}})$ to $O(N_{\mathrm{site}})$ [7]. In pure gauge systems, updates focus exclusively on plaquettes, only involving gauge configurations. When matter fields are present, horizontal and vertical links are sequentially visited to update matter and gauge configurations, after each plaquette sweep over the lattice. After completing a full lattice sweep for plaquettes and links (termed a Monte Carlo sweep), physical observables are measured using the current configuration [7].

S-3. time-dependent variational Monte Carlo for PEPS

In (1+1)D, real-time evolution methods have been successfully established using MPS within frameworks including iTEBD [23] and the time-dependent variational principle (TDVP) [24, 25]. However, in (2+1)D, the intrinsic complexity of PEPS has hindered the development of corresponding real-time evolution methods, which remains in its early stages. Therefore, in this work, we employ the time-dependent variational Monte Carlo (t-VMC) approach [26–28], which, to our knowledge, is applied here for the first time to PEPS. This method implements the TDVP and VMC for variational wave functions to compute real-time evolution. It can be understood as applying the stochastic reconfiguration method [29] to real time instead of imaginary time. The core step is to solve a system of linear equations:

$$iS_{mn}\dot{\alpha}_n = g_m, \tag{S6}$$

where S_{mn} is the overlap matrix:

$$S_{mn} = \langle O^*_m(\mathbf{s}) O_n(\mathbf{s})\rangle - \langle O^*_m(\mathbf{s})\rangle\langle O_n(\mathbf{s})\rangle. \tag{S7}$$

The solution $\dot{\alpha}_m$ of the equation system is solved by iterative conjugate gradient method. When updating the variational parameters according to the ordinary differential equation (ODE) $\frac{d}{dt}\alpha_m = \dot{\alpha}_m$, we find a first-order update by $\alpha_m(t + \Delta t) = \alpha_m(t) - \Delta t * \dot{\alpha}_m(t)$ does not work well for real-time dynamics. To overcome this problem, one can use the fourth-order Runge-Kutta method to solve the ODE. Alternatively, we use a convenient method recently proposed in Ref. [30] using Taylor expansion, sequentially updating the variational parameters twice in a time order per time step Δt according to

$$\begin{aligned} \alpha_m(t_1) &= \alpha_m(t) - c_1 * \Delta t * \dot{\alpha}_m(t), \\ \alpha_m(t + \Delta t) &= \alpha_m(t_1) - c_2 * \Delta t * \dot{\alpha}_m(t_1), \end{aligned} \tag{S8}$$

where $c_{1,2} = (1 \pm i)/2$. This gives a error $O(\Delta t^3)$ for expansions [30]. Here we use $\Delta t = 0.005$, which works very well in all cases. Apparently, for a total time $T = 18$, this needs 7200 evolution steps following Eqs.(S8).

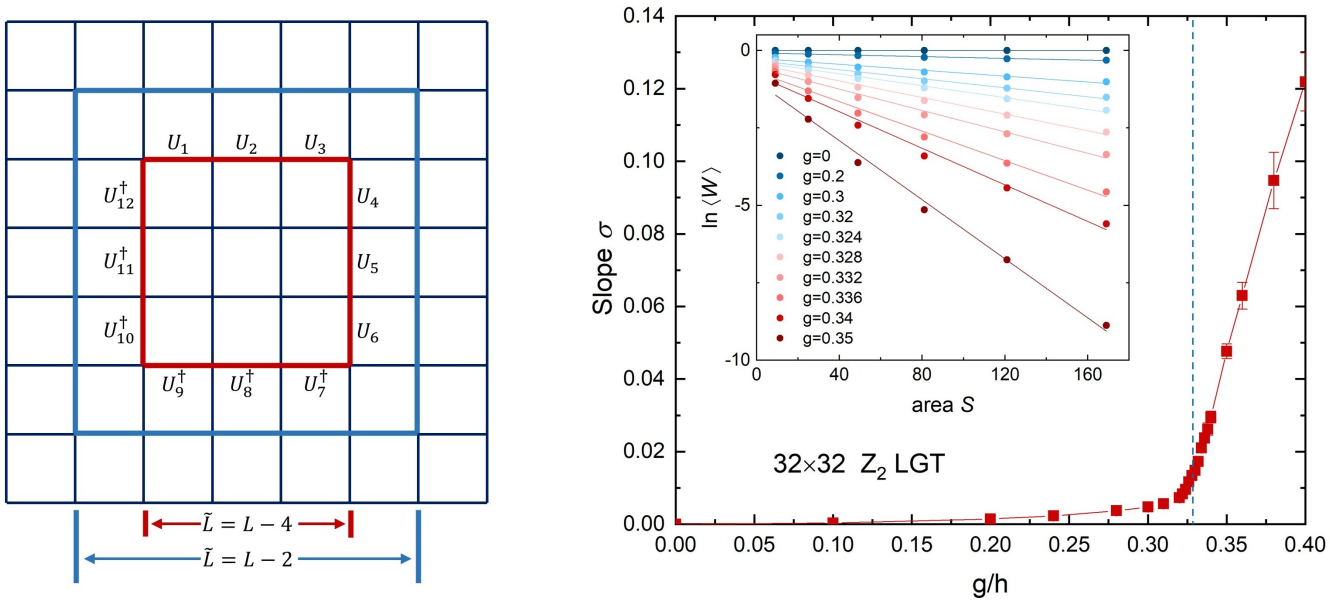

FIG. S1. Left: Computing Wilson loop operators around a central square $\tilde{L} \times \tilde{L}$ on a given open boundary square lattice $L \times L$. Two different closed paths (red and blue) are highlighted, with corresponding area $S = 9$ and $S = 25$. Right: The behavior of Wilson loop operator for $\mathbb{Z}_2$ LGT on a 32×32 lattice. The inset shows the linear fits of $\ln \langle W \rangle \propto -\sigma S$ to extracted the slope σ; the main panel shows the variation of σ with g/h increasing, and the vertical bule dashed line denotes the critical point $g_c \simeq 0.3285$ from quantum Monte Carlo [31].

TABLE I. Ground state energy per site. The top part shows QMC and GI-PEPS ($D = 4$) energy comparison for 16×16 $\mathbb{Z}_2$ LGT. The rest shows the D-convergence of GI-PEPS energy at critical points for the largest sizes, i.e. 24×24 $\mathbb{Z}_3$ LGT and 20×20 $\mathbb{Z}_4$ LGT, respectively.

$\mathbb{Z}_2$	**QMC**	**PEPS**
$g = 0.30$	$-0.76400(3)$	$-0.763973(8)$
$g = 0.31$	$-0.73841(6)$	$-0.738443(6)$
$g = 0.32$	$-0.71400(7)$	$-0.714032(8)$
$g = 0.33$	$-0.69091(7)$	$-0.690923(6)$
$g = 0.34$	$-0.6691(1)$	$-0.669161(6)$
$g = 0.35$	$-0.6486(1)$	$-0.648714(6)$
$\mathbb{Z}_3$	$D = 6$	$D = 9$
$g = 0.375$	$-0.548401(6)$	$-0.548409(4)$
$\mathbb{Z}_4$	$D = 8$	$D = 12$
$g = 0.33$	$-0.712554(8)$	$-0.712557(4)$

S-4. Additional $\mathbb{Z}_N$ LGT results.

We use $D_k = 2$ which we find is good enough for convergence on relevant sizes (see Table I) resulting in total PEPS bond dimension $D = 4$, 6, 8, respectively for $\mathbb{Z}_2$, $\mathbb{Z}_3$ and $\mathbb{Z}_4$ LGTs.

The $\mathbb{Z}_2$ LGT can be simulated unbiasedly by quantum Monte Carlo (QMC) via duality to the transverse field Ising model. Shown in Table I, near the critical point $g_c \simeq 0.3285$ [31], PEPS energies agree excellently with QMC, indicating $D_k = 2$ well converges the results. Here QMC has slightly larger uncertainties due to critical slowing-down, whereas wavefunction-based PEPS show minimal sampling uncertainties due to the zero energy variance principle for ground state, as mentioned above.

Wislon loop operator. The Wilson loop operator W is evaluated along a closed square path of dimensions $\tilde{L} \times \tilde{L}$. As illustrated in the left panel of Fig. S1 for a 3×3 lattice (red lines), this operator takes the form

$$W = U_1 \otimes \cdots \otimes U_6 \otimes U_7^\dagger \otimes \cdots \otimes U_{12}^\dagger,$$

acting on the gauge field variables along the closed contour. Its expectation value $\langle W \rangle$ can be efficiently computed

via Monte Carlo sampling. For an $L \times L$ lattice, we select a series of concentric $\tilde{L} \times \tilde{L}$ closed paths and calculate $\langle W \rangle$ for each path, where S denotes the area enclosed by the loop.

In pure $\mathbb{Z}_2$ lattice gauge theory, the Wilson loop exhibits distinct scaling behaviors across phases: perimeter-law scaling in the deconfined phase and area-law scaling in the confined phase. This transition can be quantified through the string tension σ, obtained from the scaling relation $\langle W \rangle \propto e^{-\sigma S}$. We determine σ by performing linear fittins on $\ln\langle W \rangle$ versus S, as shown in the right panel of Fig. S1 based on the 32×32 lattice. The evolution of σ with g/h clearly demonstrates a phase transition between the deconfined regime (small σ) and confined regime (large σ).

In addition, for $\mathbb{Z}_2$ gauge theory coupled to hard-core bosons, in the main text we employ different bulk region definitions to estimate thermodynamic-limit energies [7]. Specifically, the blue contour in Fig. S1(left) demarcates a central $(L-2) \times (L-2)$ region, while the red contour corresponds to a $(L-4) \times (L-4)$ region. By analyzing these progressively smaller bulk regions across varying lattice sizes $L \times L$, we perform systematic finite-size extrapolations, as shown in the main text.

S-5. Comparison with iPEPS results for $\mathbb{Z}_3$ LGT

The ground states of the $\mathbb{Z}_3$ lattice gauge theory (LGT) have been studied using the iPEPS method with a non-gauge-constrained ansatz, optimized via simple update imaginary time evolution. To benchmark our results, we compare the thermodynamic limit ground state energy obtained from our finite-size extrapolations with the corresponding iPEPS energies reported in Ref. [32].

Note that the Hamiltonian parameter g used in this work corresponds to the coupling parameter $\tilde{g}^2$ in Ref. [32] via the relation $g = (\tilde{g}^2)^2/3$ (set $h = 1$). To facilitate comparison, we extrapolate our finite-size energies to the thermodynamic limit. The inset of Fig. S2 illustrates this extrapolation procedure for the representative case $g = 0.35$. The second and third-order polynomial fits give almost same extrapolated values.

The main panel of Fig. S2 presents both the non-gauge-constrained iPEPS energies and our extrapolated thermodynamic limit energies across a range of g values. At small g, the agreement is excellent. However, for $g \geq 0.35$, our energies become lower (as exemplified for $g = 0.35$ in the inset) and exhibit a smooth variation with g. Analysis of the first and second derivatives of our energy curve indicates a phase transition at $g_c = 0.375(3)$ (see main text). This agrees well with a recent estimate of $g_c = 0.37(1)$ obtained using neural quantum states on tori up to size 10×10 [33]. In contrast, the iPEPS energies exhibit non-smooth behavior in this critical region and yield an estimated critical point at $g_c = 0.448(3)$ [32]. This discrepancy likely arises from insufficient iPEPS accuracy near the critical point.

S-6. Additional data to real-time dynamics of the 10×10 $\mathbb{Z}_2$ gauge theory

In Fig. S3, we present the total energy of the system during the real-time simulation described in the main text for the 10×10 vison dynamics in a $\mathbb{Z}_2$ gauge theory. We use two time steps $\Delta t = 0.01$ and 0.005. We see that for $\Delta t = 0.005$ (which is adopted in the main text), the energy drift is less than 0.2% during the entire time trajectory.

In Fig. S4, we present the selected plaquette values at bond dimension $D = 6$ and $D = 8$ to demonstrate the convergence with respect to the bond dimension.

* equal contribution; yantaow@iphy.ac.cn
† equal contribution; wyliu@zju.edu.cn

[1] A. W. Sandvik and G. Vidal, Variational quantum Monte Carlo simulations with tensor-network states, Phys. Rev. Lett. **99**, 220602 (2007).
[2] N. Schuch, M. M. Wolf, F. Verstraete, and J. I. Cirac, Simulation of quantum many-body systems with strings of operators and Monte Carlo tensor contractions, Phys. Rev. Lett. **100**, 040501 (2008).
[3] L. Wang, I. Pižorn, and F. Verstraete, Monte Carlo simulation with tensor network states, Phys. Rev. B **83**, 134421 (2011).
[4] P. Emonts, M. C. Bañuls, I. Cirac, and E. Zohar, Variational Monte Carlo simulation with tensor networks of a pure Z_3 gauge theory in 2+1 D, Phys. Rev. D **102**, 074501 (2020).
[5] W.-Y. Liu, S.-J. Dong, Y.-J. Han, G.-C. Guo, and L. He, Gradient optimization of finite projected entangled pair states, Phys. Rev. B **95**, 195154 (2017).
[6] W.-Y. Liu, S. Dong, C. Wang, Y. Han, H. An, G.-C. Guo, and L. He, Gapless spin liquid ground state of the spin-$\frac{1}{2}$ $J_1 - J_2$ heisenberg model on square lattices, Phys. Rev. B **98**, 241109 (2018).

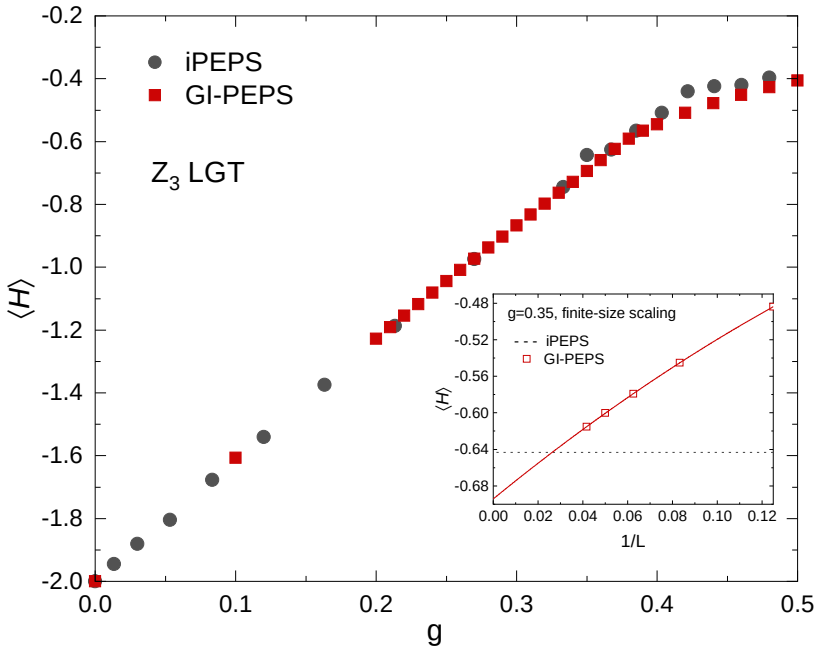

FIG. S2. Comparison of $\mathbb{Z}_3$ LGT ground state energies ($h = 1$). The inset shows the finite-size scaling of our GI-PEPS results on $L \times L$ with a second-order polynomial extrapolation including $L = 8, 12, 16, 20, 24$, and the black-dashed line denotes the iPEPS energy, at $g = 0.35$. The main panel shows the thermodynamic limit energies obtained from extrapolations of our GI-PEPS energies (extrapolation errors are about 0.0001), compared with iPEPS results taken from Ref. [32], at various g.

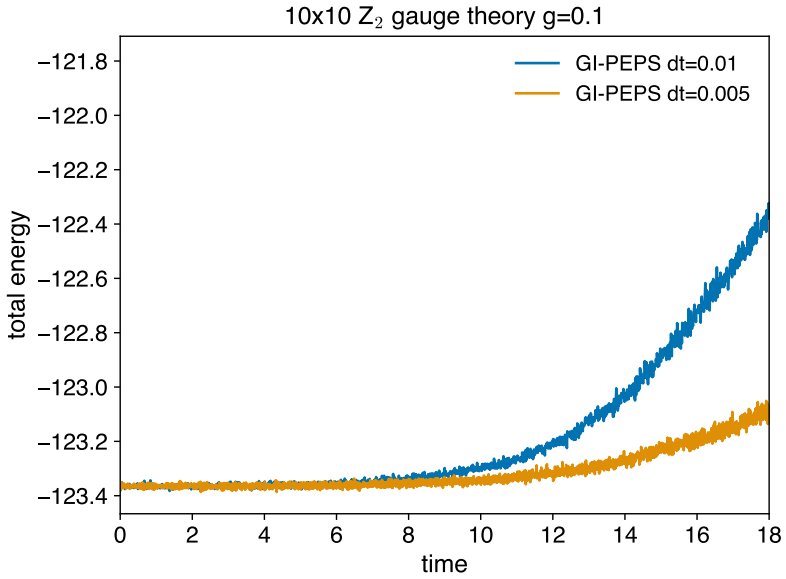

FIG. S3. Energy conservation of the vison real-time dynamics on a 10×10 $\mathbb{Z}_2$ gauge theory. The bond dimension of the GI-PEPS is 8.

[7] W.-Y. Liu, Y.-Z. Huang, S.-S. Gong, and Z.-C. Gu, Accurate simulation for finite projected entangled pair states in two dimensions, Phys. Rev. B **103**, 235155 (2021).
[8] W.-Y. Liu, S.-S. Gong, Y.-B. Li, D. Poilblanc, W.-Q. Chen, and Z.-C. Gu, Gapless quantum spin liquid and global phase diagram of the spin-1/2 $J_1 - J_2$ square antiferromagnetic Heisenberg model, Science Bulletin **67**, 1034 (2022).
[9] W.-Y. Liu, J. Hasik, S.-S. Gong, D. Poilblanc, W.-Q. Chen, and Z.-C. Gu, Emergence of gapless quantum spin liquid from deconfined quantum critical point, Phys. Rev. X **12**, 031039 (2022).
[10] W.-Y. Liu, S.-S. Gong, W.-Q. Chen, and Z.-C. Gu, Emergent symmetry in quantum phase transition: From deconfined

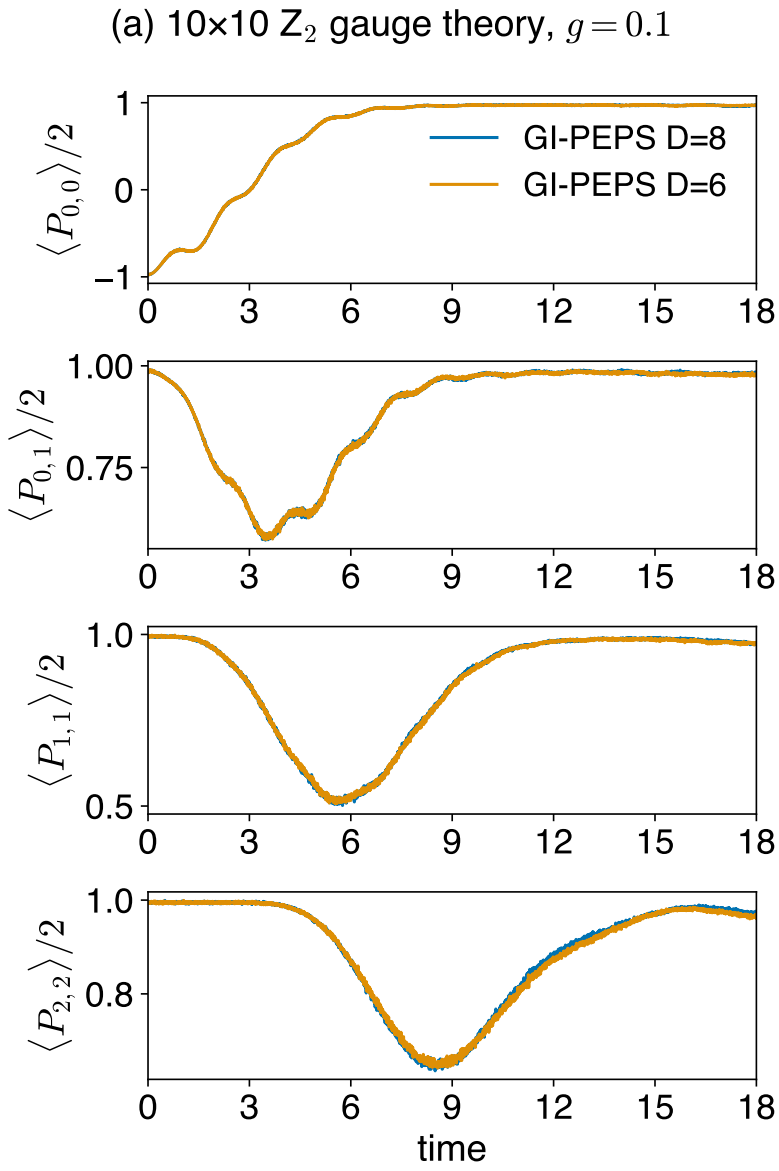

FIG. S4. Selected plaquette values of the vison real-time dynamics on a 10×10 $\mathbb{Z}_2$ gauge theory at bond dimension 6 and 8. $\Delta t = 0.005$ for both bond dimensions.

quantum critical point to gapless quantum spin liquid, Science Bulletin **69**, 190 (2024).
[11] W.-Y. Liu, D. Poilblanc, S.-S. Gong, W.-Q. Chen, and Z.-C. Gu, Tensor network study of the spin-$\frac{1}{2}$ square-lattice $J_1{-}J_2{-}J_3$ model: Incommensurate spiral order, mixed valence-bond solids, and multicritical points, Phys. Rev. B **109**, 235116 (2024).
[12] W.-Y. Liu, X.-T. Zhang, Z. Wang, S.-S. Gong, W.-Q. Chen, and Z.-C. Gu, Quantum criticality with emergent symmetry in the extended shastry-sutherland model, Phys. Rev. Lett. **133**, 026502 (2024).
[13] W.-Y. Liu, S.-J. Du, R. Peng, J. Gray, and G. K.-L. Chan, Tensor network computations that capture strict variationality, volume law behavior, and the efficient representation of neural network states, Phys. Rev. Lett. **133**, 260404 (2024).
[14] W.-Y. Liu, H. Zhai, R. Peng, Z.-C. Gu, and G. K.-L. Chan, Accurate simulation of the Hubbard model with finite fermionic projected entangled pair states, arXiv:2502.13454 (2025).
[15] S.-J. Dong, C. Wang, Y. Han, G.-c. Guo, and L. He, Gradient optimization of fermionic projected entangled pair states on directed lattices, Phys. Rev. B **99**, 195153 (2019).
[16] S.-J. Dong, C. Wang, Y.-J. Han, C. Yang, and L. He, Stable diagonal stripes in the t-J model at $\bar{n}_h = 1/8$ doping from fPEPS calculations, npj Quantum Materials **5**, 28 (2020).
[17] Y. Wu and Z. Dai, Algorithms for variational monte carlo calculations of fermion peps in the swap gates formulation (2025), arXiv:2506.20106 [cond-mat.str-el].

[18] E. Zohar and J. I. Cirac, Combining tensor networks with monte carlo methods for lattice gauge theories, Phys. Rev. D **97**, 034510 (2018).

[19] P. Emonts, A. Kelman, U. Borla, S. Moroz, S. Gazit, and E. Zohar, Finding the ground state of a lattice gauge theory with fermionic tensor networks: A $2+1d$ $\mathbb{Z}_2$ demonstration, Phys. Rev. D **107**, 014505 (2023).

[20] A. Kelman, U. Borla, I. Gomelski, J. Elyovich, G. Roose, P. Emonts, and E. Zohar, Gauged gaussian projected entangled pair states: A high dimensional tensor network formulation for lattice gauge theories, Phys. Rev. D **110**, 054511 (2024).

[21] F. Becca and S. Sorella, *Quantum Monte Carlo Approaches for Correlated Systems* (Cambridge University Press, 2017).

[22] F. Verstraete, V. Murg, and J. I. Cirac, Matrix product states, projected entangled pair states, and variational renormalization group methods for quantum spin systems, Advances in Physics **57**, 143 (2008).

[23] G. Vidal, Classical simulation of infinite-size quantum lattice systems in one spatial dimension, Phys. Rev. Lett. **98**, 070201 (2007).

[24] J. Haegeman, J. I. Cirac, T. J. Osborne, I. Pižorn, H. Verschelde, and F. Verstraete, Time-dependent variational principle for quantum lattices, Phys. Rev. Lett. **107**, 070601 (2011).

[25] J. Haegeman, C. Lubich, I. Oseledets, B. Vandereycken, and F. Verstraete, Unifying time evolution and optimization with matrix product states, Phys. Rev. B **94**, 165116 (2016).

[26] G. Carleo, F. Becca, M. Schiró, and M. Fabrizio, Localization and glassy dynamics of many-body quantum systems, Scientific Reports **2**, 243 (2012).

[27] G. Carleo, F. Becca, L. Sanchez-Palencia, S. Sorella, and M. Fabrizio, Light-cone effect and supersonic correlations in one- and two-dimensional bosonic superfluids, Phys. Rev. A **89**, 031602 (2014).

[28] K. Ido, T. Ohgoe, and M. Imada, Time-dependent many-variable variational monte carlo method for nonequilibrium strongly correlated electron systems, Phys. Rev. B **92**, 245106 (2015).

[29] S. Sorella, Green function monte carlo with stochastic reconfiguration, Phys. Rev. Lett. **80**, 4558 (1998).

[30] J. Nys, G. Pescia, A. Sinibaldi, and G. Carleo, Ab-initio variational wave functions for the time-dependent many-electron schrödinger equation, Nature Communications **15**, 9404 (2024).

[31] F. Wu, Y. Deng, and N. Prokof'ev, Phase diagram of the toric code model in a parallel magnetic field, Phys. Rev. B **85**, 195104 (2012).

[32] D. Robaina, M. C. Bañuls, and J. I. Cirac, Simulating 2+1 D $\mathbb{Z}_3$ lattice gauge theory with an infinite projected entangled-pair state, Phys. Rev. Lett. **126**, 050401 (2021).

[33] A. Apte, C. Córdova, T.-C. Huang, and A. Ashmore, Deep learning lattice gauge theories, Phys. Rev. B **110**, 165133 (2024).